Ninth International Conference on CFD in the Minerals and Process Industries
CSIRO, Melbourne, Australia
10-12 December 2012

LINEAR INSTABILITIES ON MODEL POLAR VORTICES GENERATED IN A DIFFERENTIAL-DISK ROTATION CONFIGURATION

Tony VO[1*], Luca MONTABONE[2] and Gregory J. SHEARD[1]

[1] Department of Mechanical Engineering, Monash University, Victoria 3800, AUSTRALIA
[2] Atmospheric, Oceanic and Planetary Physics, University of Oxford, Parks Road, Oxford OX13PU, UNITED KINGDOM
*Corresponding author, E-mail address: Tony.Vo@monash.edu

ABSTRACT

A numerical study on a shear layer produced via a differential-disk rotation system reveals that the flow is susceptible to instabilities under certain conditions. The incompressible Navier–Stokes equations are solved on a two-dimensional meridional semi-plane. The steady-state axisymmetric base flows demonstrate strong depth-independence and symmetry about the vertical mid-plane at low Rossby number (*Ro*) which is broken at higher *Ro*. Three-dimensional instability modes in the form of rings of vortices rearranged in a polygonal configuration extending the depth of the tank form at critical values of *Ro* and Ekman number. Differences in preferential states are observed between negative and positive *Ro*.

NOMENCLATURE

A	Shear layer aspect ratio
Ek	Ekman number
f	Coriolis parameter
H	Height
k	Azimuthal wavenumber
P	Kinematic pressure
N_p	Element polynomial degree
R_d	Disk radius
R_t	Tank radius
Ro	Rossby number
Re	Reynolds number
T	Time period
$\mathbf{u}$	Velocity vector
α	Diffusion coefficient
λ	Azimuthal wavelength
μ	Dynamic viscosity
μ_f	Floquet multiplier
ν	Kinematic viscosity
ρ	Fluid density
σ	Growth rate
Ω	Tank rotation
ω	Disk rotation relative to tank
ω_z	Axial vorticity

INTRODUCTION

Polygonal structures are widely observed in rotating flow systems. Rich examples of rotating flows are present on Earth, generated as a result of planetary rotation, and a physical understanding of these flows benefits many industrial processes. The presence of shear layers within these flows makes them susceptible to instabilities. The onset of instability causes an initially stable circular vortex structure to transition to other polygonal shapes. Striking examples of these polygonal deformations of vortices are observed in the massive polar vortices on planets, such as Saturn's hexagonal North Pole vortex and Venus' dipolar South Pole vortex. It has been proposed that these structures are a result of barotropic instability (Sommeria *et al*. 1991; Montabone *et al*. 2009; Aguiar *et al.* 2010).

Numerous simple confinements have been successful in producing similar structures observed in nature, albeit at a much smaller scale. The experimental work of Hide & Titman (1968) pioneered investigations into these rapidly rotating flows, which is important in understanding the phenomena of oceanic and atmospheric dynamics where Coriolis forces are dominant. That study comprised of a rotating circular cylinder within which a differentially rotating disk was suspended. The differential rotation of the disk produced various boundary and shear layers which become unstable at a well-defined threshold. Two dimensionless parameters are used to categorize these rotating flows, namely the Rossby number *Ro*, and Ekman number, *Ek*. The Rossby number provides a measure of inertial to Coriolis forces while the Ekman number is the ratio between viscous and Coriolis forces. Thus, Rossby and Ekman numbers much less than unity imply that rotation is highly important.

The results from Hide & Titman demonstrated a transition from axisymmetric flow to non-axisymmetric flow at a certain Rossby number threshold. As *Ro* is increased beyond this threshold, the initially circular shear layer circumscribing the disk becomes unstable and develops multiple vortices for positive Rossby numbers. Viewed along the axis of rotation, the vortices illustrate polygonal configurations. Further increases in *Ro* caused a reduction in the number of vortices down to a lower limit of two. A different phenomenon is observed for negative *Ro* whereby only an off-axis ellipse was obtained. This is in contrast with Fruh & Read (1999) who observed the transition to multiple vortex states for both negative and positive Rossby numbers.

These polygonal structures have been observed and created in a variety of differential-disk(s) rotation configurations (Rabaud & Couder 1983; Fruh & Read 1999; Aguiar *et al*. 2010), along with source-sink systems (Sommeria *et al*. 1991; Montabone *et al*. 2010), with and without the influence of varying the Coriolis parameter (Konijnenberg *et al*. 1999). The most unstable modes have been mapped onto numerous regime diagrams. Despite the differences in experimental set-ups, transition to lower modes with increasing supercriticality of a governing parameter of either *Ro*, *Re* or *Ek*, is a phenomenon

observed consistently in these shear layer experiments. In contrast to this tendency, the results of the linear stability theory on a shear layer and jet from Niino & Misawa (1984) suggested an increasing number of vortices with increasing *Re*. The model they investigated included the effects of both internal viscosity and Ekman friction, which were found to be equally important in determining the critical *Re* and the corresponding wavenumber.

This paper considers a differential rotating system which comprises a rotating cylindrical container with flow variation imparted by the differential rotation of disks occupying the inner radius of the base and lid of the cylinder. Despite previous investigations on similar systems, the numerical stability aspect has not been thoroughly detailed in a three-dimensional model. Many past numerical investigations have approximated the flow field with the quasi-geostrophic equation and have used two dimensional models (Chomaz *et al*. 1988; Bergeron *et al*. 1996; Konijnenberg *et al*. 1999). Though the simulations tend to capture the same dynamical features to those observed in the experiments, they are unable to generate the wide range of flow states (Fruh *et al*. 2003), nor to examine the vertical structure of the flow when two-dimensionality is broken.

The aim of this study is to numerically investigate the linear stability of flows produced via a differentially-rotating disk set-up using a three-dimensional model. Details of the basic flow structure and stability characteristics of both positive and negative *Ro* flows and the differences between them will be given.

METHODOLOGY

Geometric Model

The system under investigation is comprised of a closed tank of radius R_t and height H. Two disks of radius R_d are centred at the top and bottom boundaries which align with the axis of rotation of the tank. The tank and disks rotate independently at a rate of Ω and $\Omega + \omega$, respectively. The proportions of the tank are scaled to match the set-up employed by Aguiar *et al*. (2010), which had R_t = 30 cm, R_d = 15 cm and H = 10 cm. A schematic diagram of the model is illustrated in figure 1. The tank is entirely filled with a working fluid which is assumed to be incompressible and Newtonian and characterised by the kinematic viscosity $\nu = \mu / \rho$, where is μ the dynamic viscosity and ρ is the fluid density.

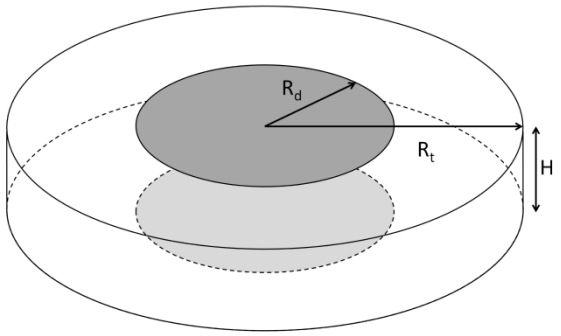

Figure 1: Schematic diagram of the differential rotating disk geometry. The shaded regions represent the disks and the white regions the tank. Relative to a laboratory reference frame, the tank rotates at a rate of Ω while the disks rotate uniformly at $\Omega + \omega$.

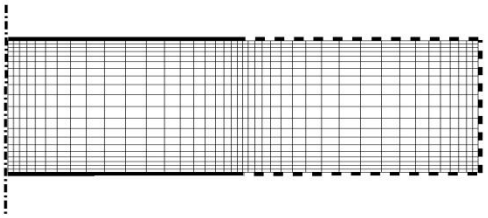

Figure 2: Two-dimensional axisymmetric mesh of an *r*-*z* semi-plane used for computations of the flow. Illustrated here are the macro elements of the discretised space. The dashed lines represent the tank boundaries which rotate at a rate of Ω, solid lines represent the disk boundaries which rotate at a rate of $\Omega + \omega$ and the dash-dot line represents the axis of rotation and spatial symmetry.

Governing Equations

The flow is governed by the unsteady incompressible Navier–Stokes equations. Lengths, velocities, time and pressure have been normalised by R_d, $R_d\Omega$, $1 / \Omega$ and $R_d\Omega^2\rho$, respectively. Thus the non-dimensional form is given by

$$\frac{\partial \boldsymbol{u}}{\partial t} + (\mathbf{u} \cdot \nabla)\mathbf{u} = -\nabla P + \frac{2EkA^2}{2-ARo}\nabla^2\mathbf{u}, \quad (1a)$$

$$\nabla \cdot \mathbf{u} = 0, \quad (1b)$$

where $\mathbf{u} = (u_z, u_r, u_\vartheta)$ is the velocity vector, P is the kinematic pressure, $A = H / R_d$ is the reciprocal shear layer aspect ratio.

It is notable that the choice of the reference quantities results in a diffusion coefficient which has a singularity and is negative for values of $Ro > 2/A$. As a consequence, only flows of $Ro < 4/3$ can be computed. Thus the selection of reference quantities has major implications for the numerical tractability of the system. An alternative scaling allows larger positive *Ro* to be explored, though that paradigm is not employed here. The Rossby number and Ekman number are defined as

$$Ro = \frac{R_d\omega}{2\bar{\Omega}H}, \quad (2)$$

$$Ek = \frac{\nu}{\bar{\Omega}H^2}, \quad (3)$$

where $\bar{\Omega} = \Omega + \omega/4$ is the mean (area-averaged) rotation rate of the disks and tank.

Numerical Treatment

The base flow is assumed to be axisymmetric and is computed on an axisymmetric meridional semi-plane which has been discretised into quadrilateral elements. The discretised mesh is shown in figure 2. The walls of the domain are solid and impenetrable with the exception of the left boundary which is treated with a symmetry boundary condition as per Blackburn & Sherwin (2004). The axis represents the axis of rotation and symmetry while the solid and dashed lines symbolise the disks and tank, respectively. There is a discontinuous jump in angular velocity across the disk-tank interface which is not modelled by an artificial forcing function such as that used by Konijnenberg *et al*. (1999). The element density of the mesh is higher in regions where boundary layers and shear layers are predicted to arise.

The Navier–Stokes equations are solved in cylindrical coordinates through a spectral-element

discretisation in space and a third-order time-integration scheme based on backward differentiation (Karniadakis *et al*. 1991). This stiffy-stable scheme has been implemented in a similar study of vortices with apparent success by Bergeron *et al*. (2000). Imposed upon each macro element are Lagrangian tensor-product polynomial shape functions. The polynomial degree N_p is varied to control spatial resolution and is interpolated at the Gauss–Lobatto–Legendre quadrature points. The present implementation in cylindrical coordinates follows work by Sheard *et al*. (2005), and was recently validated by Cogan *et al*. (2011).

Optimization of computational resource and time was examined by varying the polynomial degree imposed on each element. Convergence of three global parameters was studied: the volume integral of the azimuthal velocity relative to the tank, the magnitude of the leading eigenvalue obtained via linear stability analysis of a perturbation with azimuthal wavenumber k = 12, and the L_2 norm. Convergence of the global parameters was observed (though not shown here) with increasing N_p, and all achieved an error of 0.1% or less at N_p = 11 when compared to a higher-resolution result. Throughout the remainder of this paper a polynomial degree of 11 is employed.

Linear stability analysis

The non-axisymmetric three-dimensional structures developing on the underlying axisymmetric base flow are examined through a linear stability analysis (following Barkley & Henderson 1996; Sheard 2011). This technique allows the three-dimensional stability of individual azimuthal Fourier modes to be determined from leading eigenmodes of an evolution operator of the linearised Navier–Stokes equations.

The Navier–Stokes equations are linearised by separating the velocity and pressure fields in their respective mean and (small) perturbation. The resulting products between perturbation terms are assumed to be small and neglected. This yields a linearised equation which has a similar form to the original Navier–Stokes equations, (1a) and (1b). The difference is in the advection operator which is no longer non-linear in **u**, as shown in equation 4. The primes and bars denote the perturbation and mean values, respectively, and α is the diffusion coefficient defined as $(2EkA^2)/(2\text{-}ARo)$.

$$\frac{\partial \boldsymbol{u}'}{\partial t} + (\bar{\mathbf{u}} \cdot \nabla)\mathbf{u}' + (\mathbf{u}' \cdot \nabla)\bar{\mathbf{u}} = -\nabla P + \alpha \nabla^2 \mathbf{u}' \quad (4a)$$

$$\nabla \cdot \mathbf{u}' = 0 \quad (4b)$$

Eigenvalues from the stability analysis correspond to Floquet multipliers (μ_f) of the system which can be complex. Leading eigenvalues dictate the dominant instability mode for each azimuthal wavenumber. An implicitly restarted Arnoldi method is used to extract the leading eigenmodes of the linearised perturbation fields (Sheard 2011). The growth rate is related to the Floquet multiplier via

$$\mu_f = e^{\sigma T}, \quad (5)$$

where T is an arbitrary (due to the steady-state base flows in this study) time interval over which the equations are integrated within the eigenmode solver. Stable modes are characterised by $|\mu_f| < 1$ (negative σ) and unstable modes by $|\mu_f| > 1$ (positive σ).

Rayleigh–Kuo criterion

Rayleigh (1880) developed a necessary condition for three-dimensional instability in barotropic two-dimensional flows of constant depth. This assumes that the Coriolis parameter is constant. However, variation of the Coriolis parameter simulated by a linearly-varying depth is usually a more appropriate approximation for geophysical applications. The importance of this Coriolis variation was considered by Kuo (1949) who extended the necessary condition developed by Rayleigh (1880). In cylindrical coordinates, the condition is given by

$$\frac{\partial \omega_z}{\partial r} = \frac{\partial u_\vartheta}{\partial r^2} + \frac{1}{r}\frac{\partial u_\vartheta}{\partial r} - \frac{u_\vartheta}{r^2} - \frac{\partial f}{\partial r} = 0, \quad (5)$$

where f is the Coriolis parameter. The net result is that for barotropic instability to be possible, it is necessary that the gradient of absolute vorticity change sign somewhere within the domain.

RESULTS

Axisymmetric flow

Steady-state solutions of the base flow were obtained for numerous Rossby number and Ekman number combinations. The Rossby numbers and Ekman numbers investigated here range between $-1.0 < Ro < 0.6$ and $5\times10^{-5} < Ek < 4\times10^{-3}$. Negative and positive Rossby numbers refer to cases where the disks are rotating slower and faster than the tank, respectively.

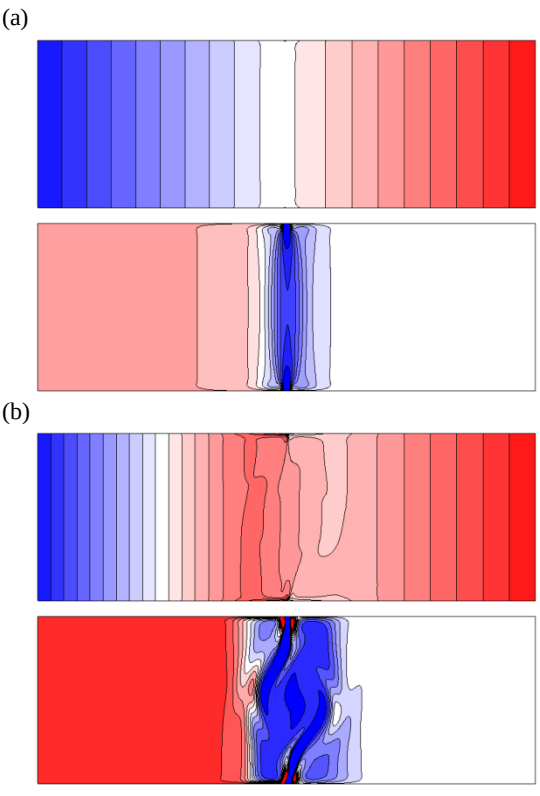

Figure 3: Contours plots of azimuthal velocity (upper frame) and axial vorticity (lower frame) for axisymmetric flows with (a) Ro = 0.05 and $Ek = 3\times10^{-4}$ and (b) Ro = 0.6 and $Ek = 3\times10^{-4}$. Blue to red contours show arbitrary low and high values, respectively.

The structure of the axisymmetric flows for a low and high *Ro* at a constant *Ek* is illustrated in figure 3. At low *Ro*, the flow demonstrates strong two-dimensionality with broad depth-independence in the interior of the tank (shown by vertical contour lines), as predicted from the Taylor–Proudman theorem (see Pedlosky, 1987). However, at higher values of *Ro*, this two-dimensionality breaks and the interior flow becomes complex in structure. Symmetry about the mid-depth axis is also broken. The highest gradients in azimuthal velocity and axial vorticity remain concentrated around the disk-tank interface, while the flow is largely uniform outside of this region. Ekman boundary layers form along the disk-tank boundaries and a vertical Stewartson layer exists at the disk-tank interface.

The observations seen for the positive *Ro* cases hold true for negative *Ro*, with the exception that the two-dimensionality is not seen to break down for the range of negative Rossby numbers investigated here. Variation of the Ekman number influences the thickness of the region over which changes in vorticity occur. A small *Ek* produces small shear layers while a large *Ek* produces thicker shear layers. The Ekman number also has demonstrated a weak dependence on the degree of two-dimensionality of the flow. A small *Ek* guides the flow towards barotropic flow. Thus results obtained for *Ro* and *Ek* much less than unity have demonstrated the predictions of the Taylor-Proudman theory. They also validate the quasi-geostrophic models used in previous studies. Ekman pumping and suction, respectively, are seen for positive and negative *Ro* at the disk-tank interface.

The Rayleigh–Kuo criterion was applied to the extracted azimuthal velocity profile at mid-depth (where barotropic flow behaviour is exhibited). The gradient of absolute vorticity for various *Ro* is shown in figure 4. The necessary condition is satisfied by all cases as every trend crosses zero at least once in the domain. The common crossing occurs at the disk-tank interface (r=1), which is where the most dynamic flow behaviour is present. This suggests the possibility of a barotropic instability developing in that vicinity.

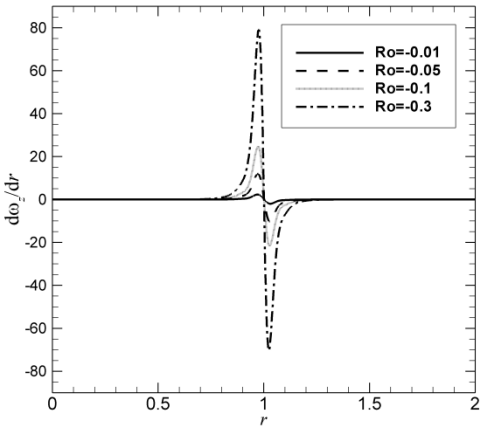

Figure 4: Gradient of axial vorticity as a function of radius for various Rossby numbers at an Ekman number of $Ek = 6\times10^{-5}$. The curves all cross the zero-line axis at least once at the disk-tank interface (e.g. at r=1). For clarity, only negative Rossby numbers are shown.

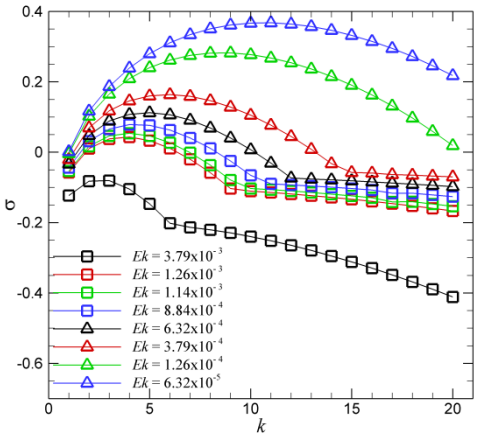

Figure 5: Growth rate σ as a function of wavenumber *k* for various Ekman numbers at *Ro* = -0.1578. The only stable flow found at this Ro is at Ek = 3.79×10-3.

Linear stability analysis

The axisymmetric steady-state flow solutions were used as a basis for the linear stability analysis. Azimuthal wavenumbers of $1 \leq k \leq 20$ are considered for a wide range of Rossby and Ekman number combinations. The wavenumber relates to the azimuthal angular wavelength λ by $k = 2\pi/\lambda$. Within this range, the fastest-growing three-dimensional mode is determined. The zeroth wavenumber is omitted as it was always found to be stable. In contrast the eigenvalues of the non-zero wavenumbers are complex which suggests that the mode is quasi-periodic. Differences in the stability between positive and negative Rossby numbers are highlighted in the following sections.

Negative Rossby number

The growth rates of each wavenumber investigated here, at a constant negative Rossby number for various Ekman numbers are shown in figure 5. Only the $Ek = 3.79\times10^{-3}$ curve has its peak growth rate under the zero-line which suggest that it is stable. Its profile comprises a local maximum at smaller wavenumbers followed by a gradually decreasing growth rate profile with increasing wavenumber. As *Ek* decreases, the initial hump expands over a wider range of wavenumbers with the peak growth rate occurring at larger wavenumbers. The most unstable wavenumber at $Ek = 1.26\times10^{-3}$ is $k = 4$, while it is $k = 11$ at $Ek = 6.32\times10^{-3}$. These trends have not been seen to differ for Rossby numbers down to $Ro = -1.0$. As the Rossby number is decreased, the magnitudes of the growth rates become larger, allowing large Ekman number flows to become unstable.

A typical perturbation field for negative Rossby numbers which has been decoupled from its base flow is illustrated in figure 6. It features two vertical bands of opposing vorticity which extends the entire depth of the tank at $r = 1$. This is in support of the results obtained from the Rayleigh–Kuo analysis. Decreases in Rossby number cause these bands of vorticity to become thinner. A three-dimensional visualisation of the instability mode generated by superposing the mode on the base flow is shown in figure 7. The $k = 4$ mode comprises a ring of axial vortices arranged in a 4-sided polygon. On either side of the vorticity ring are lower-vorticity patches. The mode structure is largely independent of depth and is only

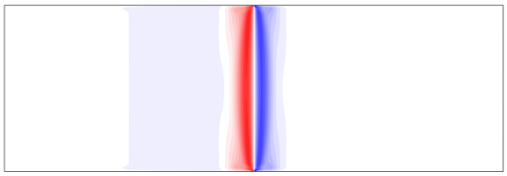

Figure 6: An isolated perturbation field of the most unstable wavenumber at (*Ro*, *Ek*) = (-0.1578, 1.26×10^{-3}). The mode is of $k = 4$. Blue to red contours show arbitrary low and high values of axial vorticity, respectively.

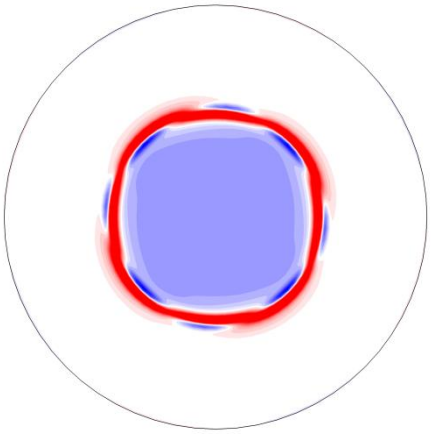

Figure 7: A perturbation field of wavenumber $k = 4$ at (*Ro*, *Ek*) = (-0.1578, 1.26×10^{-3}) which has been allowed to evolve over time on an underlying frozen base flow. The axial vorticity contours are extracted at mid-depth and the mode exhibits a 4-sided polygonal appearance.

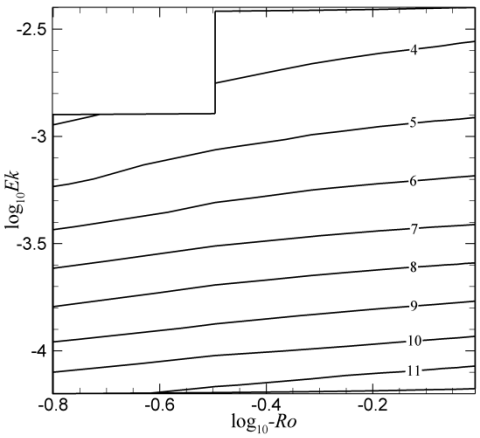

Figure 8: A *Ro*-*Ek* regime diagram of the most unstable azimuthal wavenumbers in the negative-*Ro* regime. The contours level of the curves represents the preferential mode.

observed to vary close to the horizontal boundaries, in keeping with a barotropic instability.

For the range of *Ro* and *Ek* studied here, the lowest unstable wavenumber was found to be $k = 3$. The regime diagram shown in figure 8 illustrates the dependence of the preferential modes in the *Ro*-*Ek* parameter space. It demonstrates a weak dependence on Rossby number as the contour lines remain largely horizontal at small Ekman numbers. There exists an increase in unstable mode with increasing *Ro* magnitude. This is in contrast to the experimental results of Fruh & Read (1999), who found decreasing wavenumber for increasing *Ro* magnitude. Although their system and the system studied here differ, the discrepancy is likely due to the non-linear effects in the experiment. The disagreement between linear stability and experimental results were also observed by Niino & Misawa (1984).

Positive Rossby number

Many similarities in stability characteristics are seen between negative and positive Rossby numbers. The commonalities will be briefly described and attention will focus on the differences.

The growth rate as a function of wavenumber has a similar profile seen in figure 5 for small Rossby numbers. That is, a local low-wavenumber peak followed by a decreasing growth rate with increasing wavenumber. The wavenumber of peak growth rate also increases with decreasing Ekman number. This trend is broken as *Ro* is increased. Notably evident at $Ro = 0.6$, the gradually decreasing section at higher wavenumbers begins to exhibit its own mode of instability. This is illustrated in figure 9. At large *Ek*, the initial primary peak is dominant and the resulting unstable wavenumber is low. Decreases to *Ek* lead to the high-wavenumber mode peak becoming larger in amplitude and ultimately exceeds growth rates of the small-wavenumber mode. Thus, the high wavenumber mode becomes dominant. The change of the most unstable wavenumber is dramatic and the rapid increase in wavenumber does not appear to have an upper limit. The appearance of this second instability mode may relate to the flow states referred to as chaotic in Aguiar *et al.* (2010).

At the higher Rossby numbers, the perturbation field does not illustrate long depth-independent vertical vorticity bands like those shown in figure 6. Instead, the bands are truncated and additional vorticity structures are observed throughout the flow. Axial vorticity contours of an evolved perturbation coupled with the base flow is shown in figure 10. Lower-level vorticity is seen to circumscribe the triangular inner vortex. The structure depicted here varies throughout the depth of the tank.

Though not shown here, the positive-*Ro* parameter space exhibits dominant unstable wavenumbers varying from $k = 2$ to 7 for low-wavenumbers and $k = 17$ to 40 for

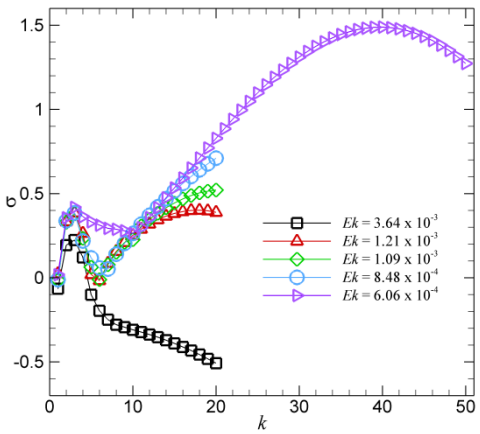

Figure 9: Growth rate σ as a function of wavenumber k for various Ekman numbers at $Ro = 0.6$. All curves shown are unstable. Two peaking structures of σ are present.

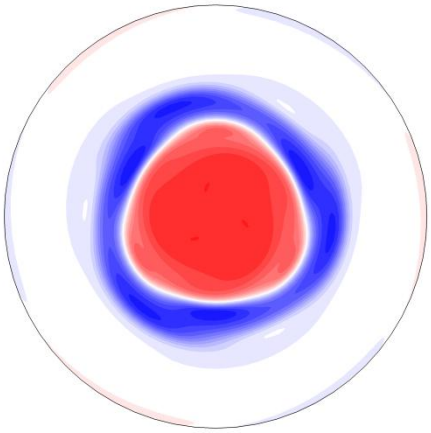

Figure 10: A perturbation field of wavenumber k = 3 superposed on the base flow at (Ro, Ek) = (0.6, 3.64×10^{-3}). The axial vorticity contours are extracted at mid-depth and the mode represents a triangle-like configuration.

high wavenumbers. It might be possible to simulate unstable wavenumbers from k = 8 to 16 with particular Ro and Ek combinations. Comparisons with modes obtained in Aguiar *et al*. (2010) illustrate differences which again, may be attributed to the differences between linear and non-linear flow states.

CONCLUSION

The linear stability of a differential-disk rotating flow has been explored for a range of Ekman numbers over both positive and negative Rossby number. As positive Ro is increased, the depth-independence becomes disturbed. Consequently, the instability modes which develop vary in structure with depth. For the range of negative Ro explored, the flow maintains a high degree of depth-wise two-dimensionality.

For positive and negative Ro, linear stability analysis predicts that decreases in Ek leads to higher unstable wavenumbers. A single mode peak in growth rate as a function of wavenumber is seen to grow in amplitude for negative Ro. A similar trend is seen for small positive Ro. However, at higher Ro, a second mode becomes dominant at higher wavenumbers.

REFERENCES

AGUIAR, A.C.B, READ, P.L., WORDSWORTH, R.D., SALTER, T. & HIRO YAMAZAKI, Y., (2010), "A laboratory model of Saturn's North Polar Hexagon". *Icarus*, **206** (2), 755–763.

BERGERON, K., COUTSIAS, E.A., LYNOV, J.P. & NIELSEN, A.H., (1996), "Self-organization in circular shear layers". *Physica Scripta*, **67**, 33–37.

BERGERON, K., COUTSIAS, E.A., LYNOV, J.P. & NIELSEN, A.H., (2000), "Dynamical properties of forced shear layers in an annular geometry". *Journal of Fluid Mechanics*, **402** (1), 255–289.

BLACKBURN, H.M. & SHERWIN, S.J., (2004), "Formulation of a Galerkin spectral element–Fourier method for three-dimensional incompressible flows in cylindrical geometries". *Journal of Computational Physics*, **197** (2), 759–778.

CHOMAZ, J.M., RABAUD, M., BASDEVANT, C. & COUDER, Y., (1988), "Experimental and numerical investigation of a forced circular shear layer". *Journal of Fluid Mechanics*, **187** (1), 115–140.

COGAN, S.J., RYAN, K. & SHEARD, G.J., (2011), "Symmetry breaking and instability mechanisms in medium depth torsionally driven open cylinder flows". *Journal of Fluid Mechanics*, **672**, 521–544.

FRUH, W.G., NIELSEN, A.H., (2003), "On the origin of time-dependent behaviour in a barotropically unstable shear layer". *Nonlinear Processes in Geophysics*, **10** (3), 289–302.

FRUH, W.G. and READ, P.L., (1999), "Experiments on a barotropic rotating shear layer. Part 1. Instability and steady vortices". *Journal of Fluid Mechanics*, **383**,143–173.

HIDE, R. and TITMAN, C.W, (1967), "Detached shear layers in a rotating fluid". *Journal of Fluid Mechanics*, **29** (01), 39–60.

KARNIADAKIS, G.E., ISRAELI, M. & ORSZAG, S.A., (1991), "High-order splitting methods for the incompressible Navier-Stokes equations". *Journal of Computational Physics*, **97** (2), 414–443.

Van de KONIJNENBERG, JA, NIELSEN, AH, JUUL RASMUSSEN, J. & STENUM, B., (1999), "Shear-flow instability in a rotating fluid". *Journal of Fluid Mechanics*, **387**, 177–204.

KUO, H., (1949), "Dynamic instability of two-dimensional nondivergent flow in a barotropic atmosphere". *Journal of Meteorology*, **6**, 105–122.

Journal of Atmospheric Sciences 6, 105–122.

MONTABONE, L., WORDSWORTH, R., AGUIAR, A., JACOBY, T., McCLIMANS, T., READ, P.L & WILSON, C., (2009), "Coherent structures in planetary polar vortices: A laboratory view". In *International Conference on Comparative Planetology: Venus-Earth-Mars*, ESTEC, Noordwijk, Netherlands, May 11-15.

MONTABONE, L., WORDSWORTH, R., AGUIAR, A., JACOBY, T., READ, PL., MCCLIMANS, T. & ELLINGSEN, I., (2010), "Barotropic instability of planetary polar vortices: CIV analysis of specific multi-lobed structures". In *Proceedings of the HYDRALAB III Joint User Meeting, Hannover*.

NIINO, H. and MISAWA, N., (1984), "An experimental and theoretical study of barotropic instability". *Journal of Atmospheric Sciences*, **41**, 1992–2011.

PEDLOSKY, J., (1987), "Geophysical fluid dynamics". *Springer*.

RABAUD, M. and COUDER, Y., (1983), "Shear-flow instability in a circular geometry". *Journal of Fluid Mechanics*, **136**, 291–319.

RAYLEIGH, L., (1880), "On the stability, or instability, of certain fluid motions". *Proceedings of the London Mathematical Society*, **1** (1), 57.

SHEARD, G.J., (2011), "Wake stability features behind a square cylinder: Focus on small incidence angles". *Journal of Fluids and Structures*, **27**, 734–742.

SHEARD, G.J., THOMPSON, M.C. & HOURIGAN, K., (2005), "Subharmonic mechanism of the mode C instability". *Physics of Fluids*, **17**, 111702.

SOMMERIA, J., MEYERS, S.D. & SWINNEY, H.L., (1991), "Experiments on vortices and Rossby waves in eastward and westward jets". *Nonlinear Topics in Ocean Physics*, **109**, 227–269.

